Electronic Supplementary Information For

Self-healing, luminescent metallogelation driven by synergistic metallophilic and fluorine-fluorine interactions

Kalle Kolari,[a] Evgeny Bulatov,[a] Rajendhraprasad Tatikonda,[a] Kia Bertula,[b] Elina Kalenius,[a] Nonappa,[*b,c] and Matti Haukka[*a]

[a.] *Department of Chemistry, University of Jyväskylä, P. O. Box 35, FI-40014 Jyväskylä, Finland. E-mail. matti.o.haukka@jyu.fi*
[b.] *Department of Applied Physics, Aalto University School of Science, Puumiehenkuja 2, FI-02150 Espoo, Finland. E-mail. nonappa@aalto.fi*
[c.] *Department of Bioproducts and Biosystems, Aalto University School of Chemical Engineering, Kemistintie 1, FI-02150 Espo, Finland.*

Table of Contents

Experimental section

General considerations

2,6-bis(2-pyridyl)-4(1H)-pyridone, K_2CO_3, 18-crown-6, 1-iodododecane and $^{1}H,^{1}H,^{2}H,^{2}H,^{3}H,^{3}H$-perfluoroundecyl iodide were purchased from Sigma Aldrich. K_2PtCl_4 for starting material synthesis was purchased from Alfa Aesar. Ethanol produced by Altia OYJ was 95% in purity and DMSO was purchased from Merck. Uvasol grade DMSO (Merck) was used for all optical measurements. Reagents were used as received. Ligand **L1**[1] and starting material $[Pt(DMSO)_2Cl_2]$[2] were synthesized according to literature procedures. Accurate mass values for ligand **2,** compounds **1** and **2** were measured with Agilent 6560 ESI-IM-Q-TOF mass spectrometer equipped with dualESI source. Spectroscopic measurements were done with Cary 100 UV-Vis spectrophotometer and Varian Cary Eclipse Fluorescence Spectrophotometer. ^{1}H, ^{13}C, and ^{19}F NMR spectra were recorded with Bruker Avance III HD 300 MHz. Chemical shifts are reported in parts per million (ppm, δ). ^{1}H and ^{13}C spectra were referenced to residual solvent signals. KF in D_2O was used as spectral reference for all ^{19}F spectra. ^{19}F spectral reference was measured separately and obtained spectral reference value was used in spectra calibration. IR spectroscopy was performed with the Bruker Alpha spectrometer with the ATR platinum diamond compartment.

Synthesis of 4´-(dodecyl)-2,6-bis(2-pyridyl)-4(1H)-pyridonate (L2)

0.5 mmol of 2,6-bis(2-pyridyl)-4(1H)-pyridone, 1.5 mmol K_2CO_3 and 16-crown-6 in 30 ml of acetone was stirred for 1h at room temperature. 0.5 mmol of 1-iodododecane in acetone was added dropwise to reaction mixture in 30 mins and was refluxed for 2 days. After reflux, 20 mL of water was added to reaction mixture and product was extracted with 2 x 20 ml of CH_2Cl_2 and dried under vacuum. Yield: 118 mg, 80 %. ^{1}H NMR ($CDCl_3$), δ: 0.86 (tr, 3H, J=7,1 Hz), 1.27 (d, 16H, J=14,4 Hz), 1.50 (m, 2H), 1.85 (m, 2H), 4.22 ppm (tr, 2H, J=6.5 Hz), 7.30 (dd, 2H, J=1.1 Hz), 7.32 (dd, 2H, J=1.0 Hz), 7.83 (td, 2H, J=1.75 Hz), 8.01 (s, 1H), 8.60 (d, 2H, J=7.95 Hz), 8.68 (dd, 2H, J=0.8 Hz). ^{13}C NMR ($CDCl_3$), δ: 14.09, 22.67, 25.95, 29.57, 29.62, 31.91, 68.24, 107.42, 121.33, 123.72, 136.73, 149.10, 156.25, 157.04,

167.39. HR-MS (ESI-QTOF-MS): [**L2**+H]$^+$ calculated for $C_{27}H_{36}N_3O^+$ *m/z* 418.2853, found *m/z* 418.2850.

{[Pt(L1)Cl]Cl} (1)[3]

Suspension of [$Pt(DMSO)_2Cl_2$] (0.14 mmol) in methanol (24 ml) was prepared. Dissolve equimolar amount (0.14 mmol) of L1 in 36 ml of THF and add ligand solution dropwise into methanolic suspension of [$Pt(DMSO)_2Cl_2$]. Stir reaction mixture overnight. Collect formed yellowish precipitate and evaporate the filtrate slowly to obtain yellow crystals for structure determination with x-ray crystallography. Combine crystals and precipitate then wash with 10 ml of acetone. Dry the product overnight in vacuum. Yellow crystals formed from slow evaporation of reaction mixture are instable in room temperature due to evaporation of solvent of crystallization. Yield is 72%. ^{1}H NMR (DMSO-*d6*), δ: 2.16 (t, 2H), 2.27 (quint, 2H, J=1.8 Hz), 4.51 (tr, 2H, J=5.9 Hz), 7.96 (m, 2H), 8.52 (td, 2H, J=1.2 Hz), 8.67 (d, 2H, J=7.2), 8.96 (d, 2H, J=5.3 Hz). MS (ESI-QTOF) m/z:940 [$C_{26}H_{16}N_3O_1F_{17}Cl_1Pt$]$^+$. HR-MS (ESI-QTOF-MS): [**L1**PtCl]$^+$ calculated for $C_{26}H_{16}N_3OF_{17}ClPt^+$ *m/z* 940.0350, found *m/z* 940.0367.

{[Pt(L2)Cl]Cl} (2)[3]

Ligand L2 (0.14 mmol) in 34 mL of THF is added directly to suspension of [$Pt(DMSO)_2Cl_2$] (0.14 mmol) in methanol (24 ml). Reaction mixture was stirred overnight and evaporated to dryness in vacuum. Filter the product and wash with 10 ml of cold acetone. Dry the product in vacuum overnight. Crystallization is performed from saturated hot ethanolic solution. Yield is 75%. ^{1}H NMR (DMSO-*d6*), δ: 0.85 (tr, 2H, J=6.9 Hz), 1.24 (m, 10H), 1.49 (tr, 2H, J=6.9 Hz), 1.86 (tr, 2H, J=6.4 Hz), 4.37 (tr, 2H, J=5.7 Hz), 7.93 (tr, 2H, J=6.2 Hz), 8.30 (s, 1H), 8.51 (tr, 2H, J=7.5 Hz), 8.66 (d, 2H, J=7.7 Hz), 8.88 (d, 2H, J=5.2 Hz). HR-MS (ESI-QTOF-MS): [**L2**PtCl]$^+$ calculated for $C_{27}H_{35}N_3OClPt^+$ *m/z* 648.2109, found *m/z* 648.2106.

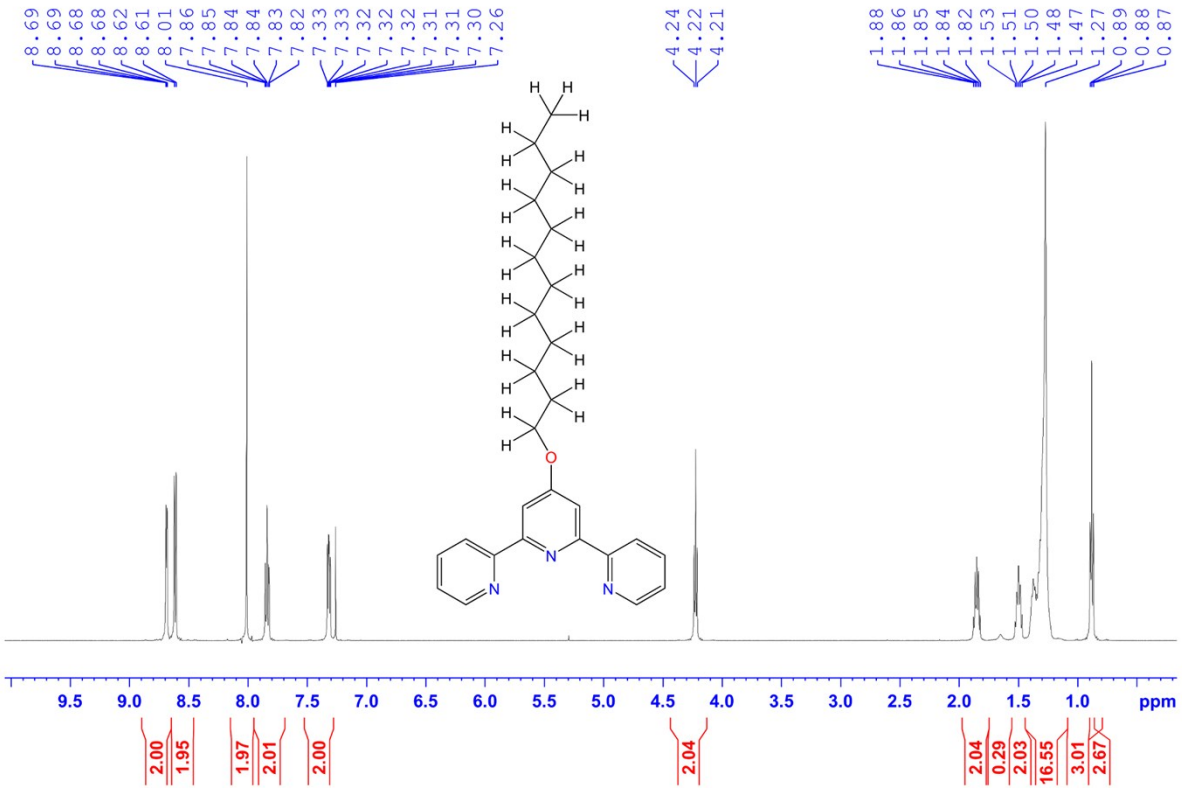

Figure S1. ^{1}H NMR of **L2** in $CDCl_3$

Figure S2. ^{13}C NMR of **L2** in $CDCl_3$

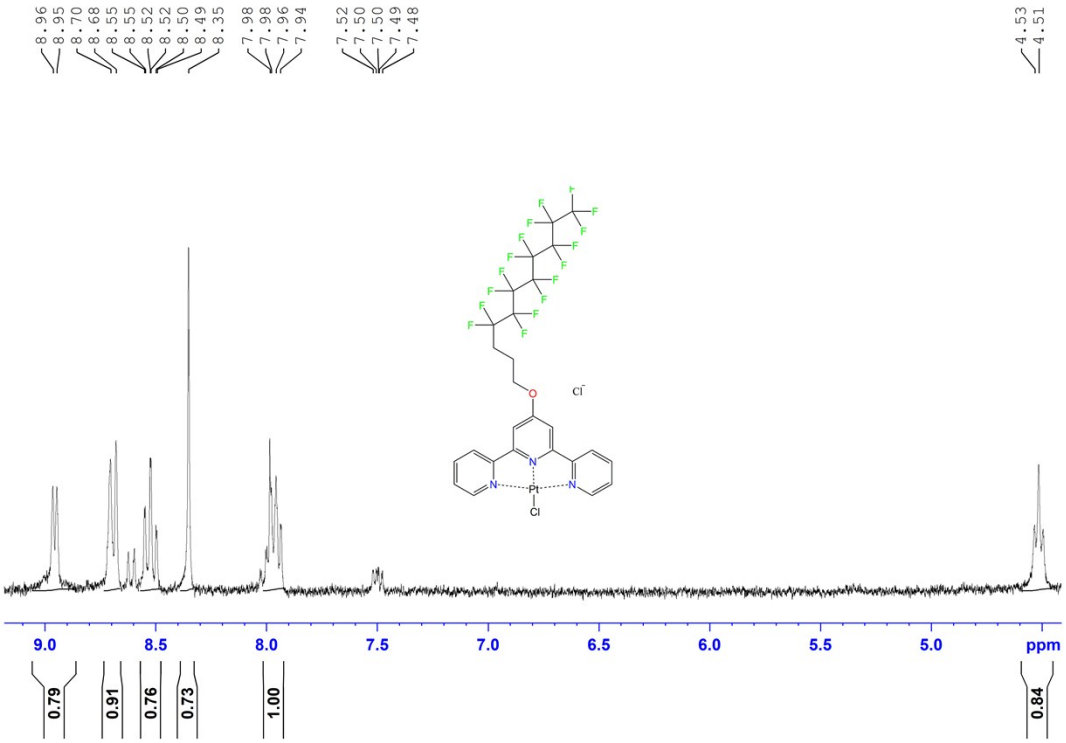

Figure S3. [1]H NMR of compound **1** in d_6-DMSO

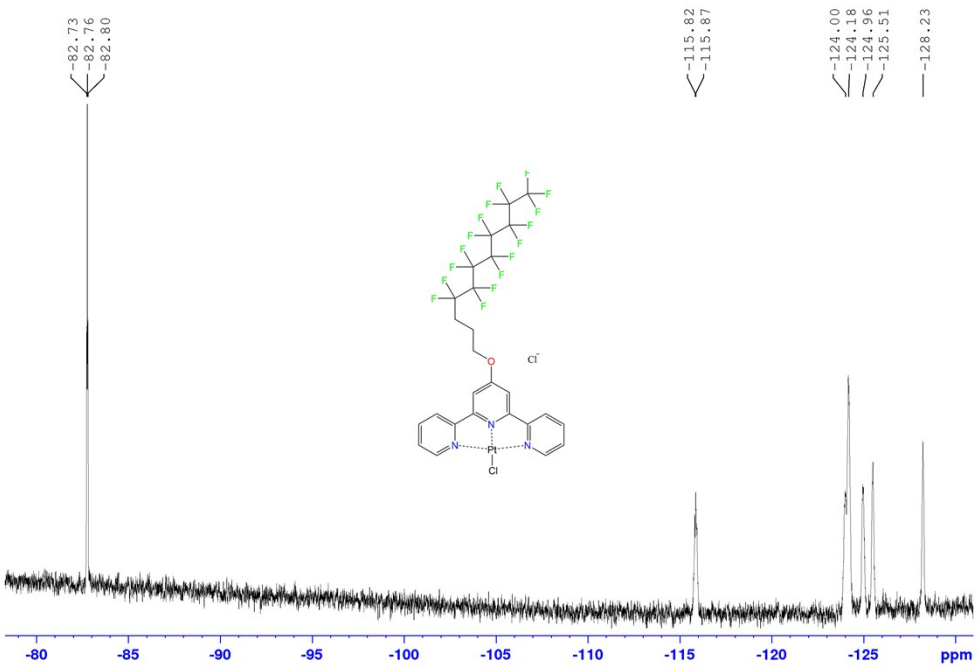

Figure S4. [19]F NMR of compound **1** in d_6-DMSO

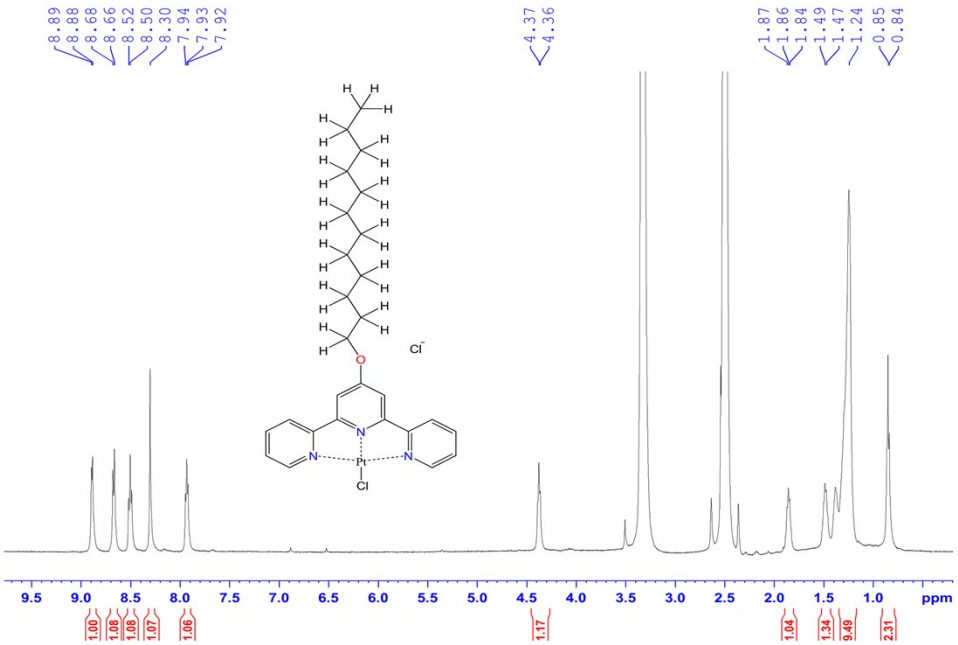

Figure S5. ^{1}H NMR of compound **2** in d_6-DMSO

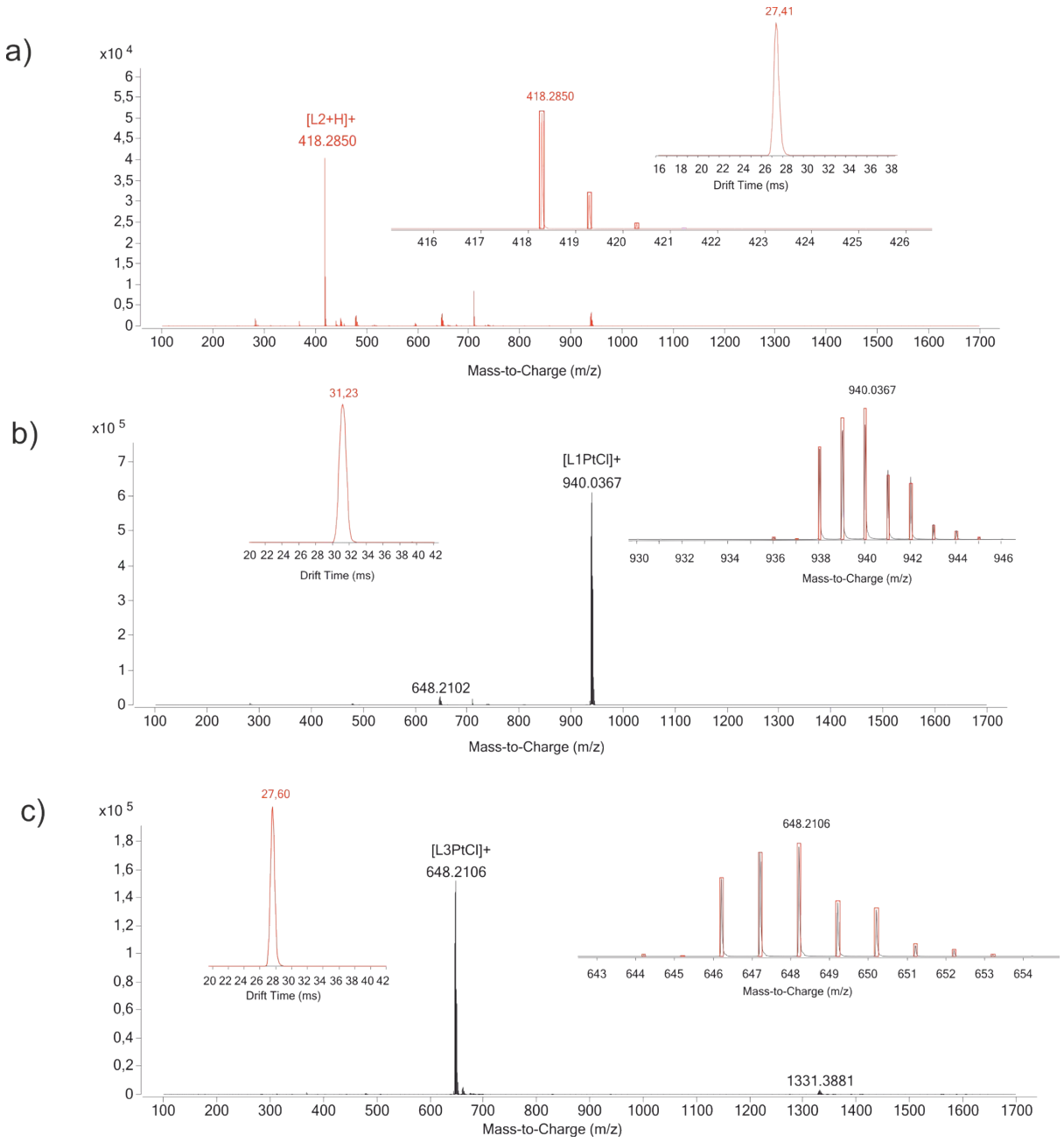

Figure S6. (+)ESI-QTOF-MS spectra measured MeCN for ligand **2** (a) and compounds **1** (b) and **2** (c). Insets show fit to theoretical isotopic distributions (red boxes) and DTIM-drift spectra (N_2 drift gas).

X-ray Crystallography

Single crystal X-ray structure determination: The crystals of **1** and **2** were immersed in cryo-oil, mounted in a MiTeGen loop and measured at 120 K. The X-ray diffraction data were collected on an Agilent Technologies Supernova diffractometer using Mo Kα radiation (λ = 0.70173 Å, compound **1**) Or Cu Kα radiation (λ = 1.54184 Å, compound **2**) The CrysAlisPro[4] program package was used for cell refinements and data reductions. The structures were solved by charge flipping method using the SUPERFLIP[5] program or by direct methods using SHELXS-2014[6] program. An empirical absorption

correction based on equivalent reflections (CrysAlisPro)[4] was applied to all data. Structural refinements were carried out using SHELXL-2014[6] with the Olex2[7] and SHELXLE[6] graphical user interfaces. For compounds **1** and **2** hydrogens were positioned geometrically and constrained to ride on their parent atoms. For compound **1** with C–H = 0.84–0.99 Å, Uiso = 1.2–1.5 Ueq (parent atom) and compound **2** C–H = 0.85–0.98 Å and Uiso = 1.2–1.5 Ueq (parent atom). Hydrogens for the solvent molecules of **1** and **2** were located from the difference fourier map and refined isotropically.

Table S1. Crystallographic data for **1** and **2**

	1	**2**
CCDC No	1949029	1949030
empirical formula	$C_{30}H_{28}Cl_2F_{17}N_3O_3Pt_1$	$C_{33}H_{53}Cl_2N_3O_4Pt_1$
fw	1067.54	821.77
temp (K)	120(2)	120(2)
λ(Å)	0.71073	1.54184
cryst syst	Triclinic	Triclinic
space group	P-1	P-1
a (Å)	7.4767(3)	7.42120(10)
b (Å)	11.6730(4)	12.1297(2)
c (Å)	21.5145(12)	20.0591(3)
α (deg)	96.026(4)	82.0460(10)
β (deg)	90.715(4)	86.2770(10)
γ (deg)	98.636(3)	85.498(2)
V (Å^3)	1845.35(14)	1780.09(5)
Z	2	2
ρ_{calc} (Mg/m^3)	1.921	1.533
μ(Mo Kα) (mm^{-1})	4.070	9.058
No. reflns.	14344	37889
Unique reflns.	6981	7445
GOOF (F^2)	1.046	1.043
R_{int}	0.0511	0.0700
R1[a] ($I \geq 2\sigma$)	0.0530	0.0375
R2[b] ($I \geq 2\sigma$)	0.1065	0.0977

[a] $R1 = \Sigma||F_o| - |F_c||/\Sigma|F_o|$. [b] $wR2 = [\Sigma[w(F_o^2 - F_c^2)^2]/ \Sigma[w(F_o^2)^2]]^{1/2}$.

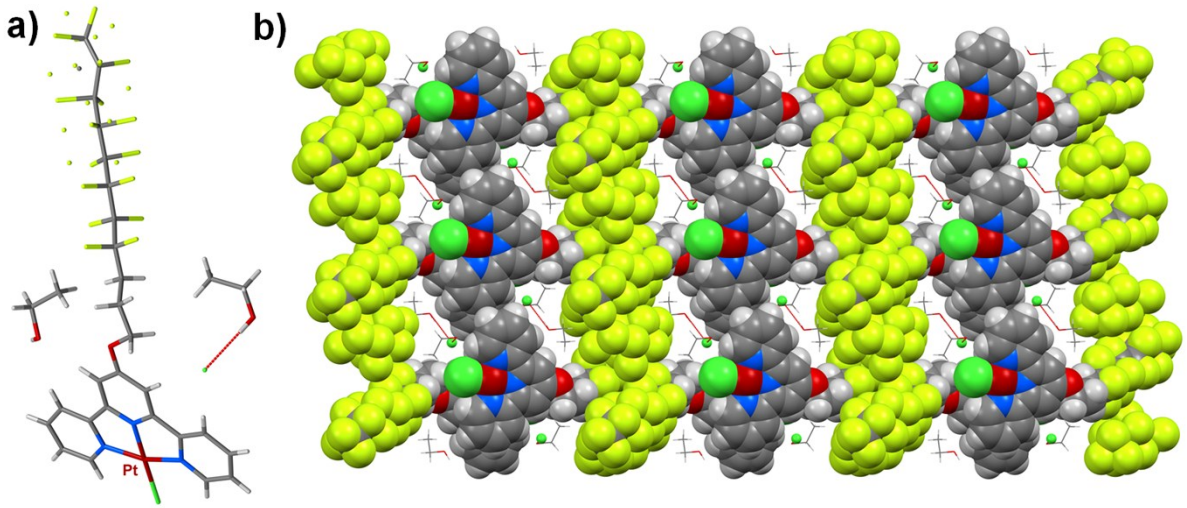

Figure S7. a) Asymmetric unit of compound **1**. b) Crystal packing along the a-axis where the voids are filled with chloride anion and ethanol solvent molecules.

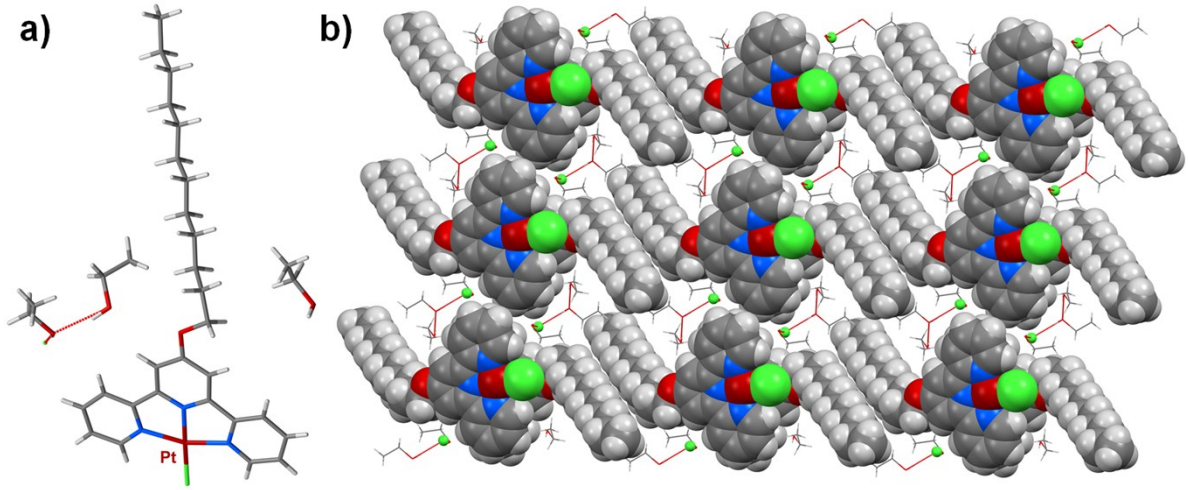

Figure S8. a) Asymmetric unit of compound **2**. b) Crystal packing along the a-axis where the voids are filled with chloride anion and ethanol solvent molecules.

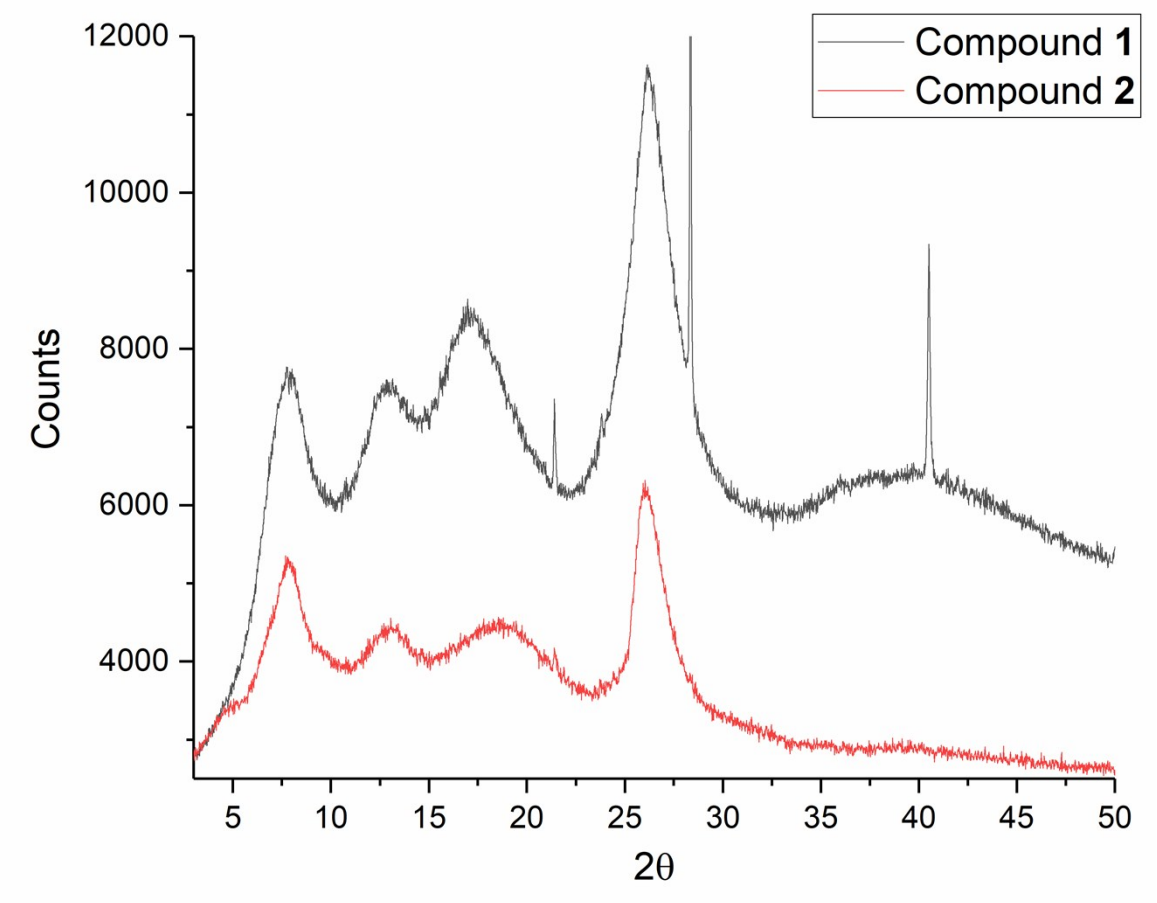

Figure S9. Powder diffractogram of compounds **1** and **2** in orange form. Compound **1** contains traces of KCl

Optical measurements

Gels for optical measurements were prepared in 1 cm quartz luminescence cuvettes using Uvasol grade DMSO solvent (Merck). Absorption and luminescence spectra of the gels were measured using Cary 100 UV-Vis and Varian Cary Eclipse Fluorescence spectrophotometers accordingly, and the temperature of the gels was varied between 25 and 99 °C using a cuvette holder connected to Omron E5CSV temperature controller.

Solid samples for optical measurements were pressed between two quartz plates. Reflectance and luminescence spectra of the solids were measured using Elmer Perkin Lambda 850 spectrophotometer equipped with 150 mm integrating sphere and Cary Eclipse Fluorescence spectrophotometer accordingly.

Emission lifetimes of the gels were measured using time-correlated single photon counting technique with PicoQuant HydraHarp 400 data acquisition system. The samples were excited at 483 nm with a diode laser head LDH-P-C-485 at a repetition frequency of 2.5 MHz driven by the PDL 800-B driver (PicoQuant GmbH), and the emitted light was collected by optic fiber and passed through a grating monochromator set to 600 nm into single photon avalanche photodiode detector (MPD). No polarizers were used in the optical path. The lifetimes were estimated by fitting the experimental data with bi-exponential model. No significant variation in the lifetimes were observed between the gels of **1** with concentrations 0.3 – 1.5 %.

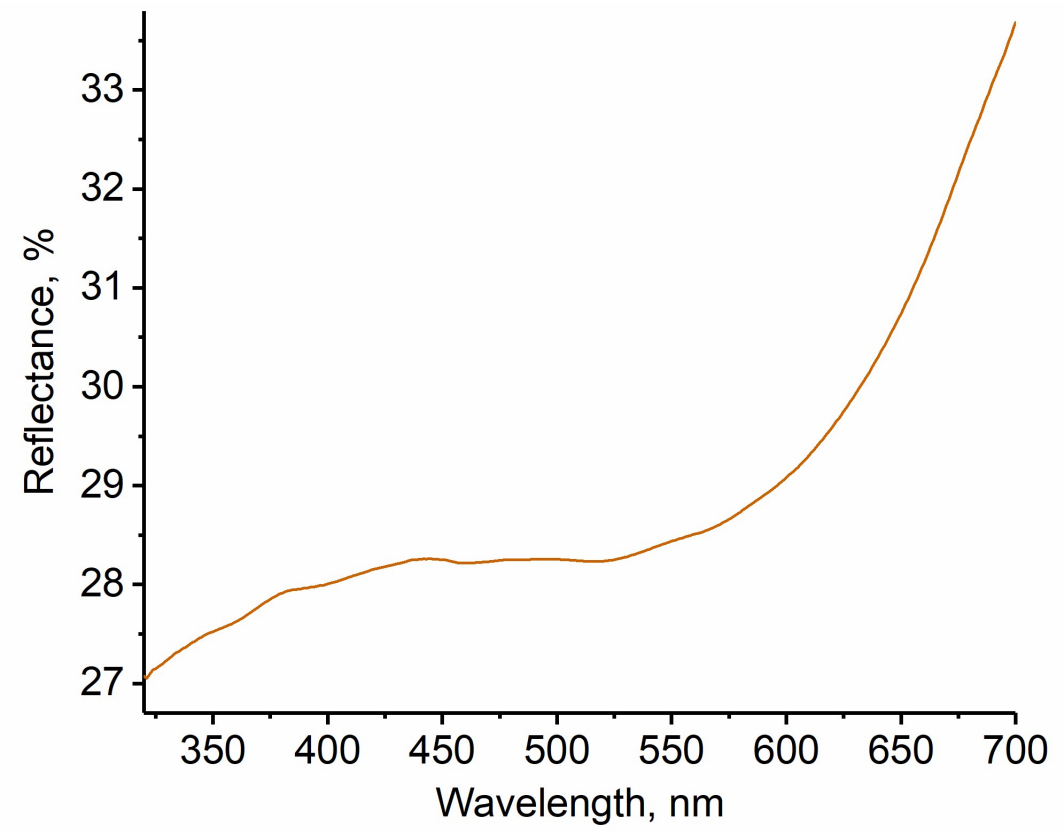

Figure S10. Reflectance spectrum of vacuum dried powder of compound **1**

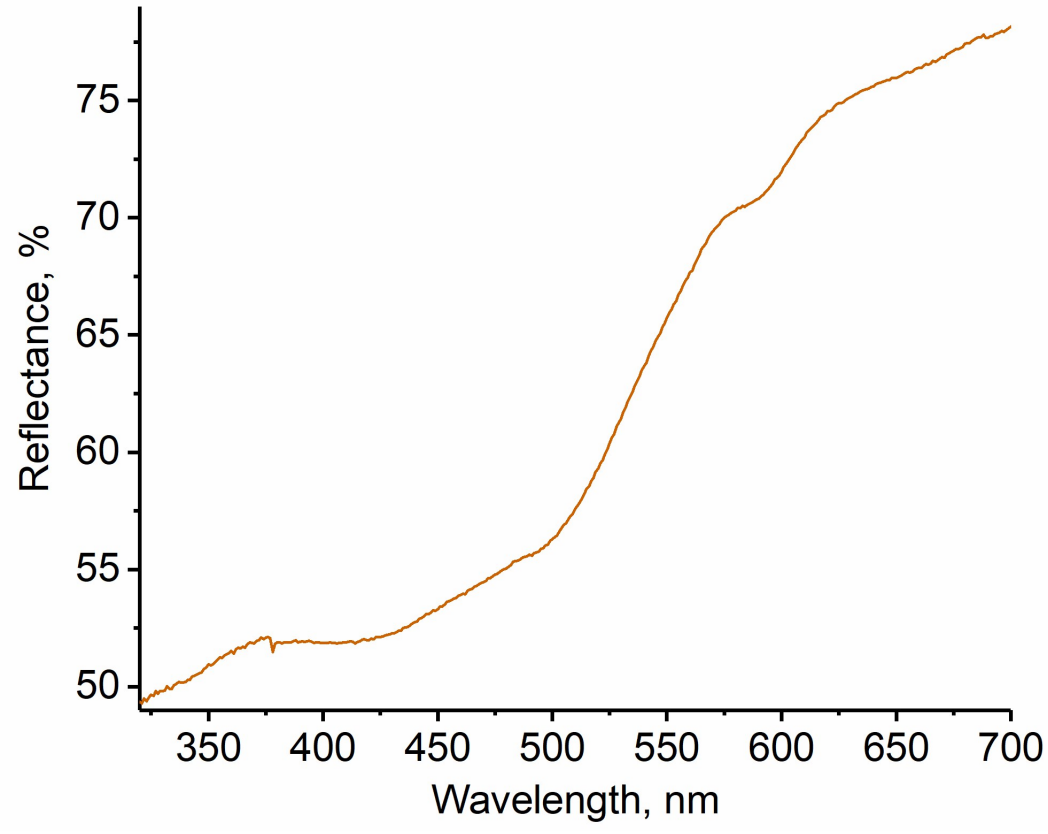

Figure S11. Reflectance spectrum of vacuum dried powder of compound **2**

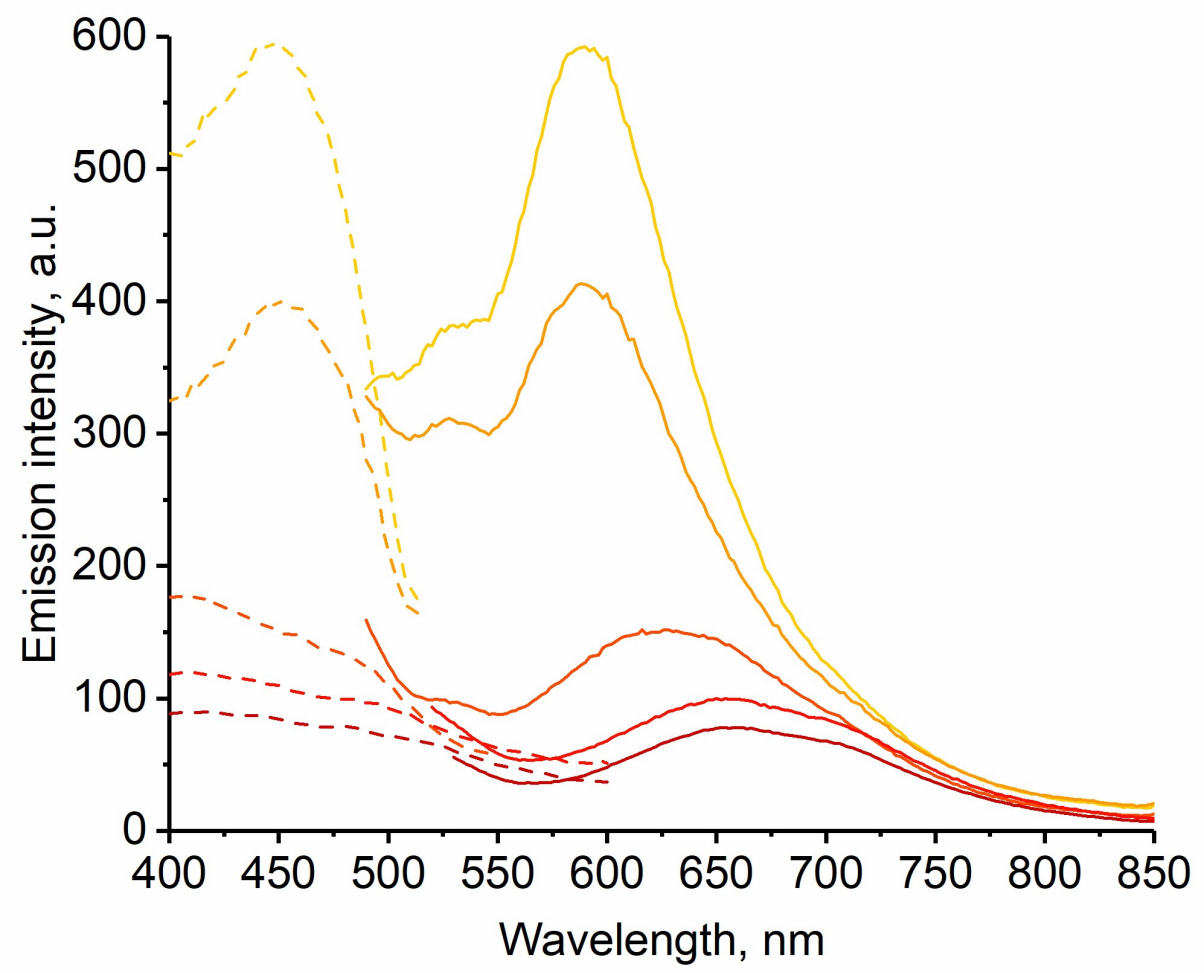

Figure S12. The red shift and decrease in emission intensity of compound **1** in solid state upon transformation from yellow to orange form.

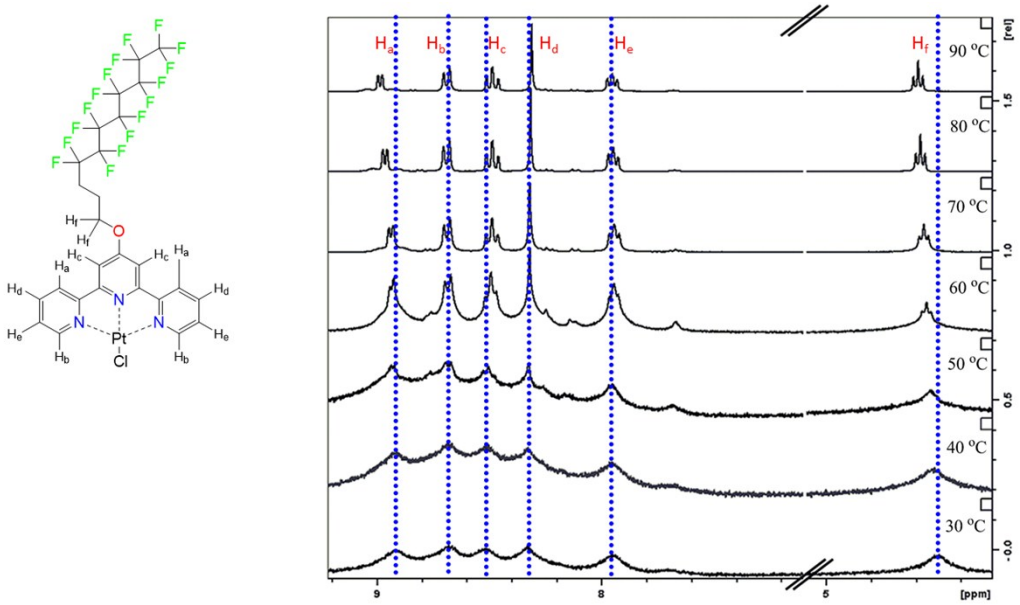

Figure S13a. Variable temperature ^{1}H NMR of 1.0 % gel of **1** in d_6-DMSO

Table **S2**. Chemical shift values (in ppm) ^{1}H VT NMR of 1.0 % DMSO-d_6 gel of **1**.

[1]H	30°C	40°C	50°C	60°C	70°C	80°C	90°C	Dd (90-30)
a	8.92	8.92	8.94	8.93	8.94	8.96	8.99	0.07
b	8.68	8.69	8.69	8.69	8.69	8.69	8.69	0.01
c	8.52	8.52	8.52	8.49	8.49	8.49	8.49	0.03
d	8.34	8.34	8.34	8.32	8.32	8.32	8.31	0.03
e	7.96	7.96	7.98	7.95	7.94	7.94	7.95	0.01
f	4.5	4.53	4.54	4.55	4.57	4.58	4.59	0.09

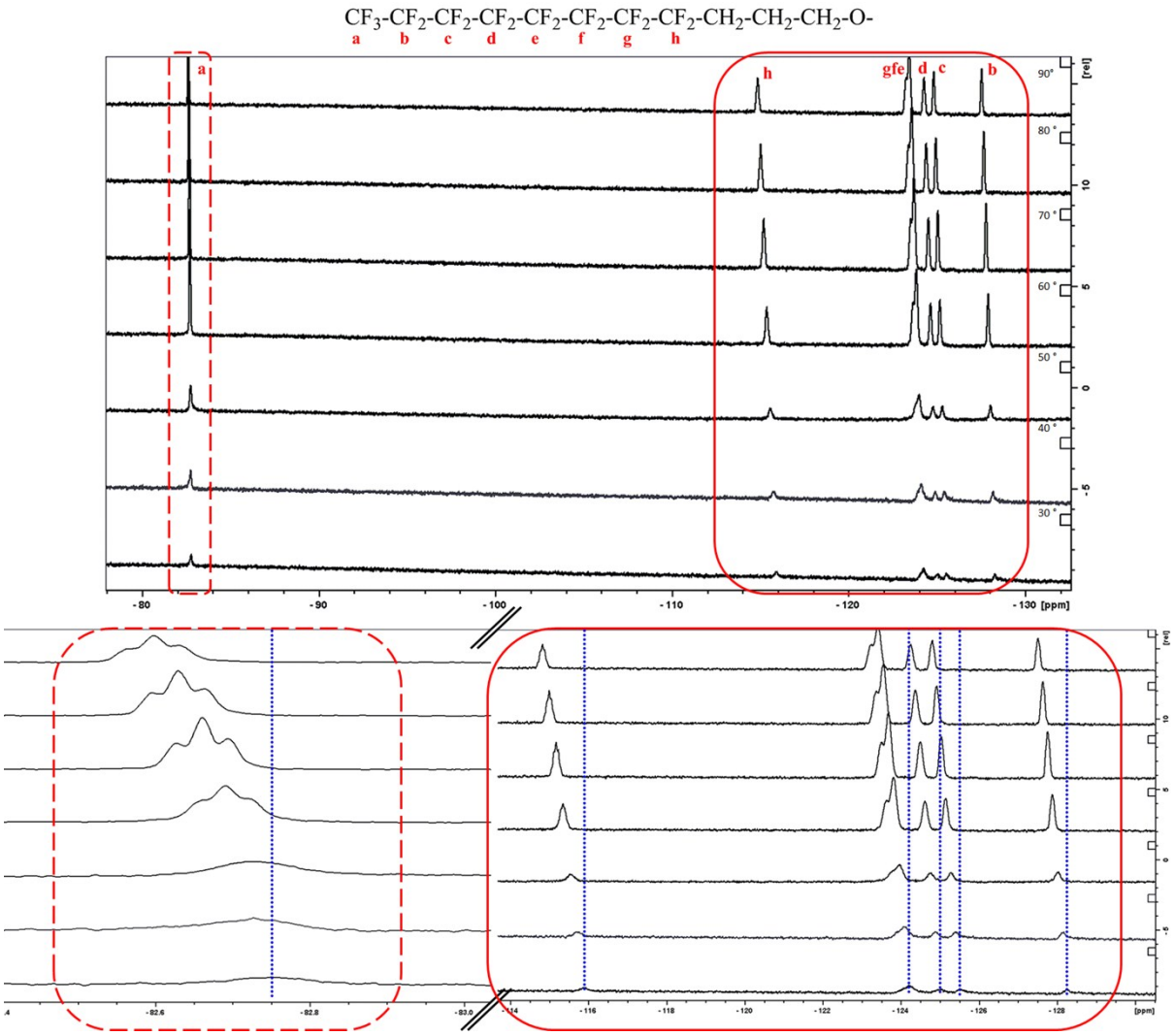

Figure S13b. Variable temperature ^{19}F NMR of 1.0 % gel of **1** in d_6-DMSO

Table **3.** Chemical shift values (in ppm) from ^{19}F VT NMR of 1.0 % gel of **1** d_6-DMSO

^{19}F	30°C	40°C	50°C	60°C	70°C	80°C	90°C	30°C (dil.sol)	Dd(90-30)	
a	-82.75	-82.73	-82.72	-82.69	-82.66	-82.63	-82.60	-82.76	0.15	
b	-128.24	-128.14	-128.02	-127.88	-127.76	-127.63	-127.51	-128.23	0.73	
c	-125.51	-125.39	-125.28	-125.16	-125.03	-124.92	-124.80	-125.51	0.71	
d	-125.03	-124.87	-124.76	-123.81	-123.68	-123.55	-123.42	-124.18	1.61	
g				-124.62	-124.50	-124.37	-124.25	-124.96	0.34	(90-60)
fe	-124.21	-124.10	-123.95	-123.65	-123.51	-123.37	-123.24	-124.0	0.97	
h	-115.89	-115.70	-115.54	-115.35	-115.17	-115.0	-114.83	-115.87	1.06	

Fluorophilic interactions and infra-red (IR) spectroscopy

Fluorophilic attraction between perfluorinated alkyl chains is associated with attractive dipole-dipole interactions between CF_2 moieties. Chains with 7 or more CF_2 groups feature strong hydrophobic and aggregation properties due to efficient packing of spiral chains, which is also observed in the crystal structure of **1** (**Figure 1d** and **S8b**).[8,9]

Fluorophilic interactions in **1** appear vital for gel formation, since alkyl-substituted **2** possesses non-gelling behavior. In order to study the contribution of fluorophilic interaction in aggregation and gelation of **1**, IR absorption spectra of the solid orange form, gel, and concentrated solution of **1** were measured (**Figure S15**).

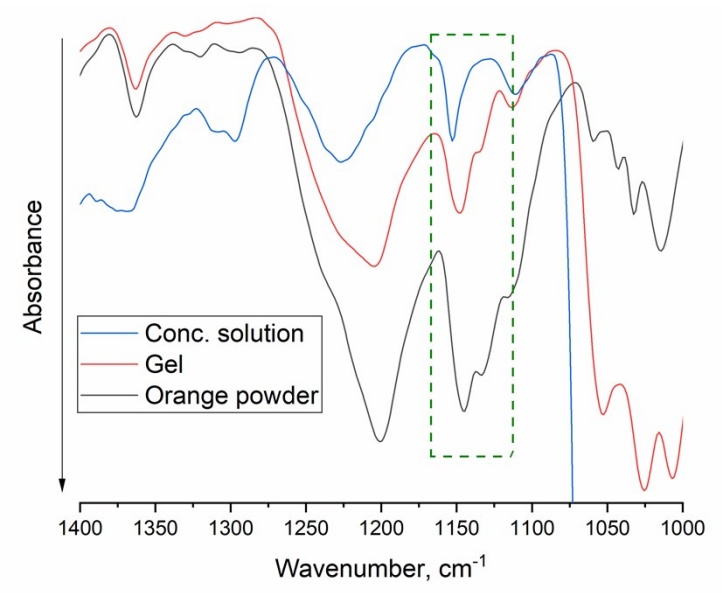

Figure S14. Normalized and baseline-adjusted IR absorption spectra of complex **1** in solid, gel (1%) and concentrated solution (0.4%).

Symmetric stretching vibration of CF_2 groups ($\nu_s(CF_2)$) gives rise to a characteristic absorption band in IR spectrum, position of which depends on length of the perfluoroalkyl chain and the extent of fluorophilic aggregation. For $(CF_2)_7$ chain the wavenumber of 1146.7 cm^{-1} has been reported in close packing (the strongest aggregation), which shifts to higher wavenumbers with weaker fluorophilic interactions.[9,10] In agreement with the reported data, the orange powder of **2** possesses absorption peak at 1144 cm^{-1}, which shifts to 1148 cm^{-1} in gel state, and further to 1153 cm^{-1} in solution, indicating gradual weakening of the fluorophilic interactions. Therefore, the obtained IR spectra clearly indicate the presence of fluorophilic interactions in the gel of complex **1**.

Scanning Electron Microscopy (SEM)

The sample preparation for SEM was performed by preparing 1.0 % metallogel in a 4 mL vial. Gels were then freezed using liquid propane and vaccum dried to obtain aerogels samples. Aerogel samples were placed on the carbon tape sticked to an aluminium stubb and the samples were then sputter coated with 4 nm iridium using Leica EM ACE600 high vacuum sputter coater. SEM micrographs were imaged with a Zeiss Sigma VP scanning electron microscope (acceleration voltage 1.5 kV).

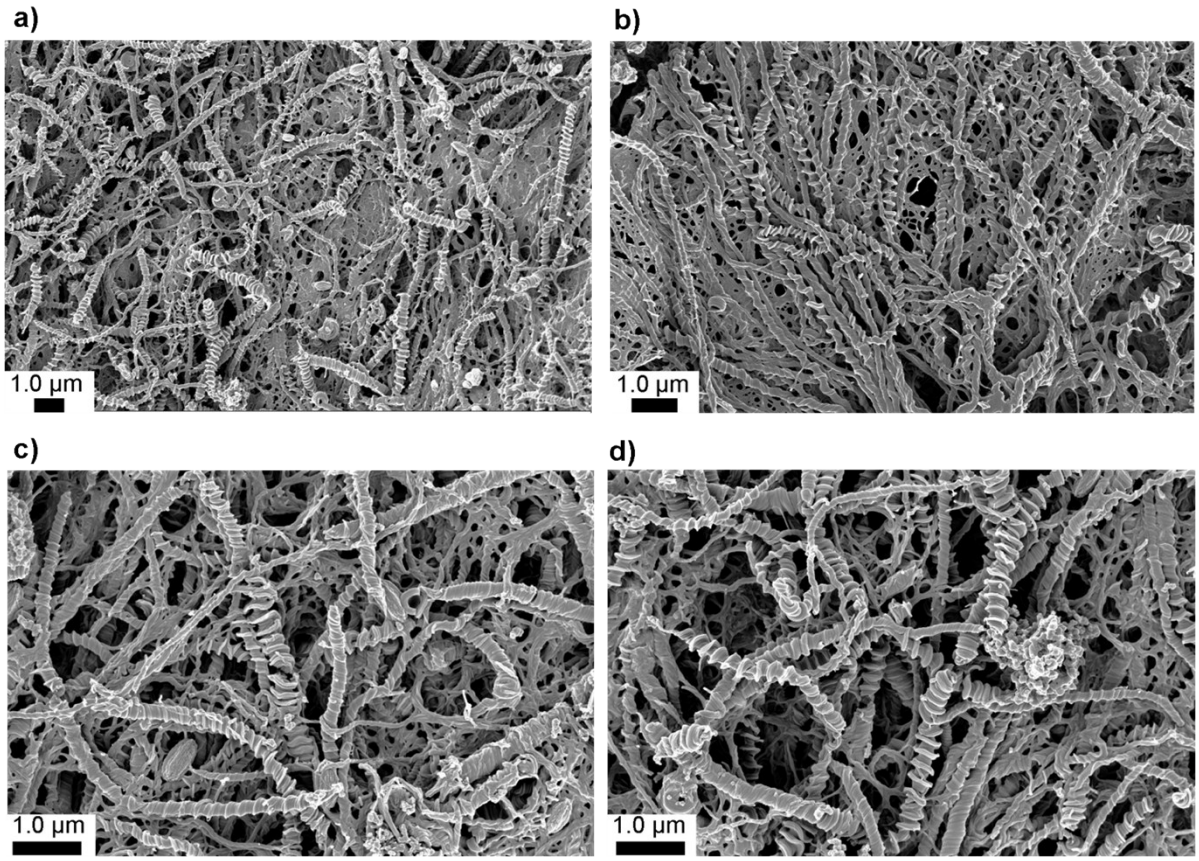

Figure S15. Scanning electron microscopy. SEM micrographs of aerogels obtained from 1.0 % DMSO gel of **1.**

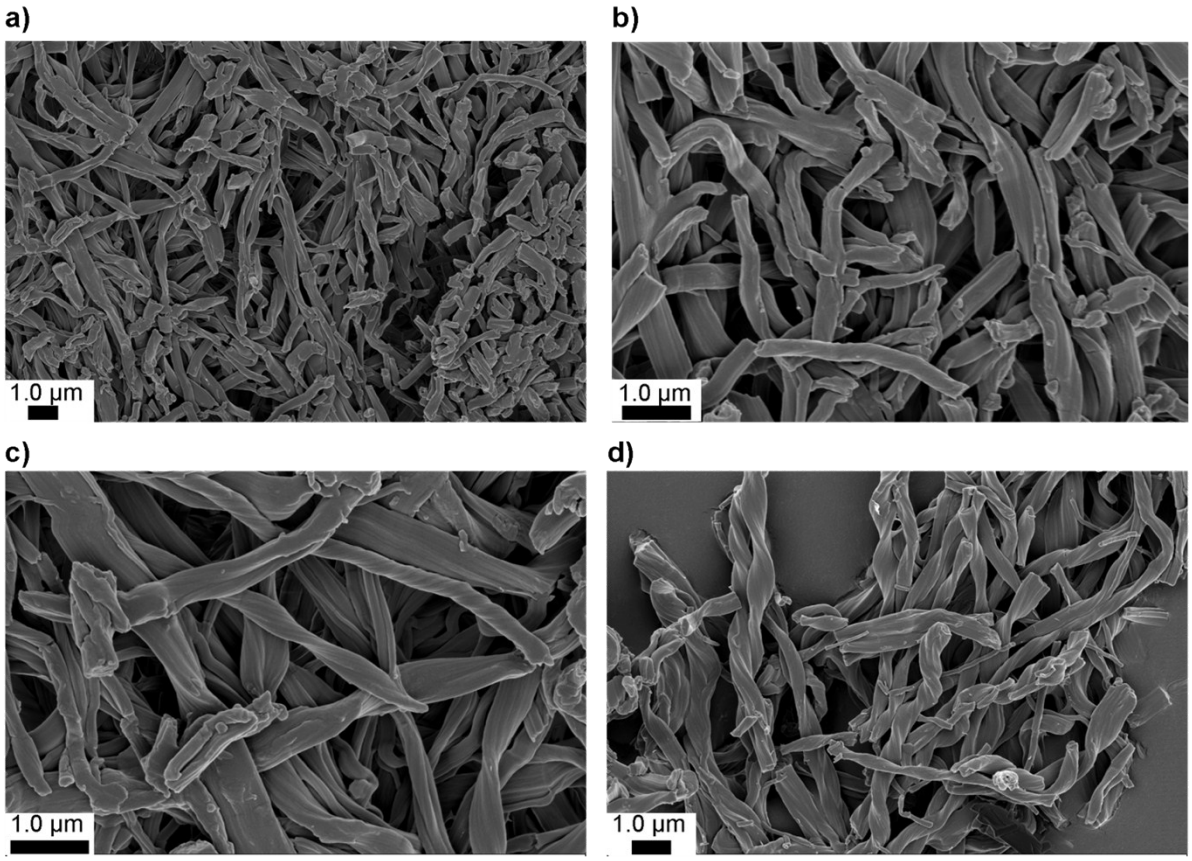

Figure S16. Scanning electron microscopy. SEM micrographs of aerogels obtained from 1.0 % DMF gel of **1.**

Transmission Electron Microscopy (TEM)

The transmission electron microscopy (TEM) images were collected using FEI Tecnai G2 operated at 120 kV and JEM 3200FSC field emission microscope (JEOL) operated at 300 kV in bright field mode with Omega-type Zero-loss energy filter. The images were acquired with GATAN digital micrograph software while the specimen temperature was maintained at -187 ^{o}C. The TEM samples were prepared by drop casting 5.0 μL of the gel on to a 300 mesh copper grid with lacey carbon support film. The excess sample was removed by blotting with Whatman® filter paper. The samples were dried under ambient condition for 48 hours prior to imaging.

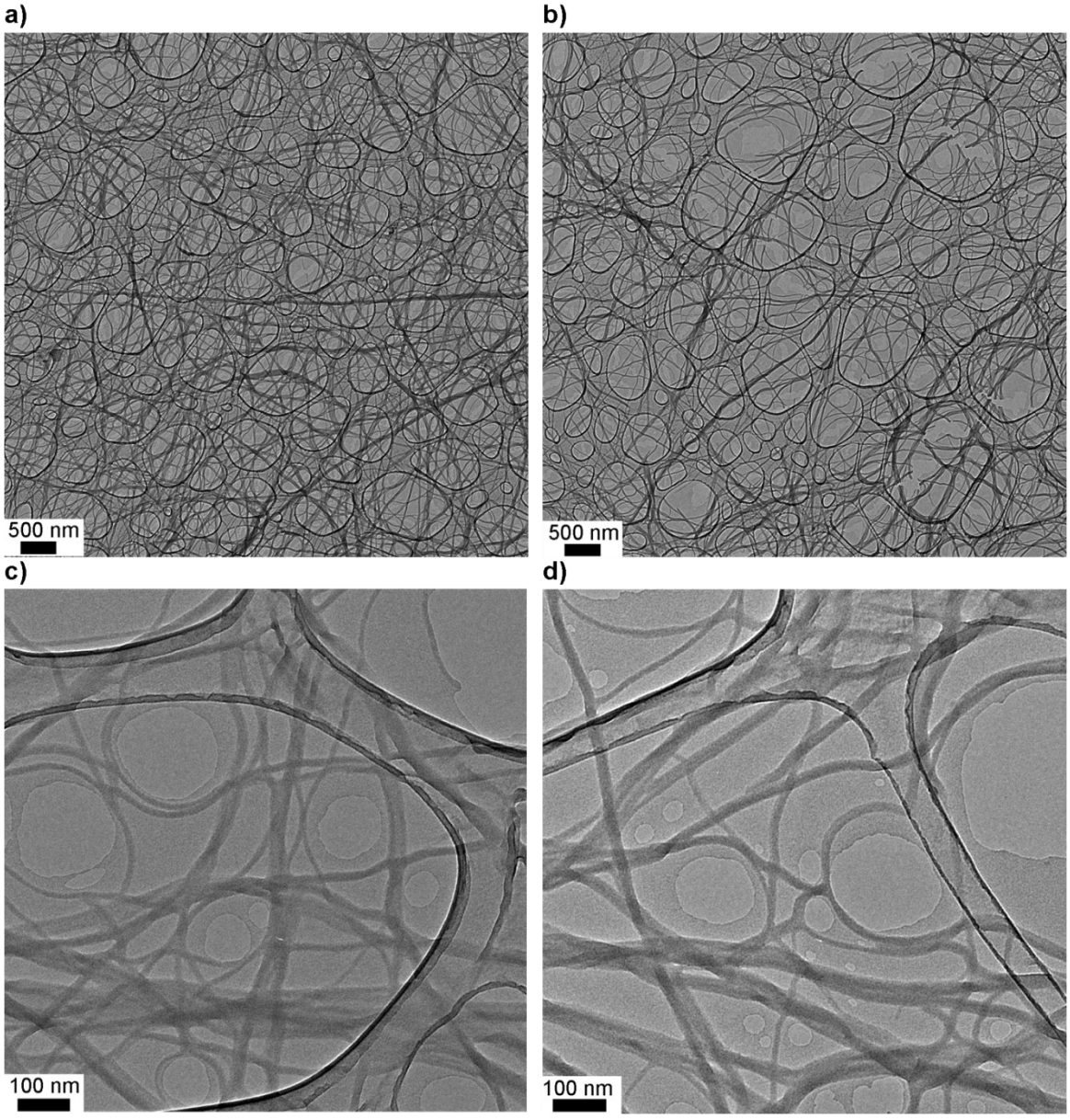

Figure S17. Transmission electron microscopy. TEM micrographs of aerogels obtained from 1.0 % DMSO gels of **1.**

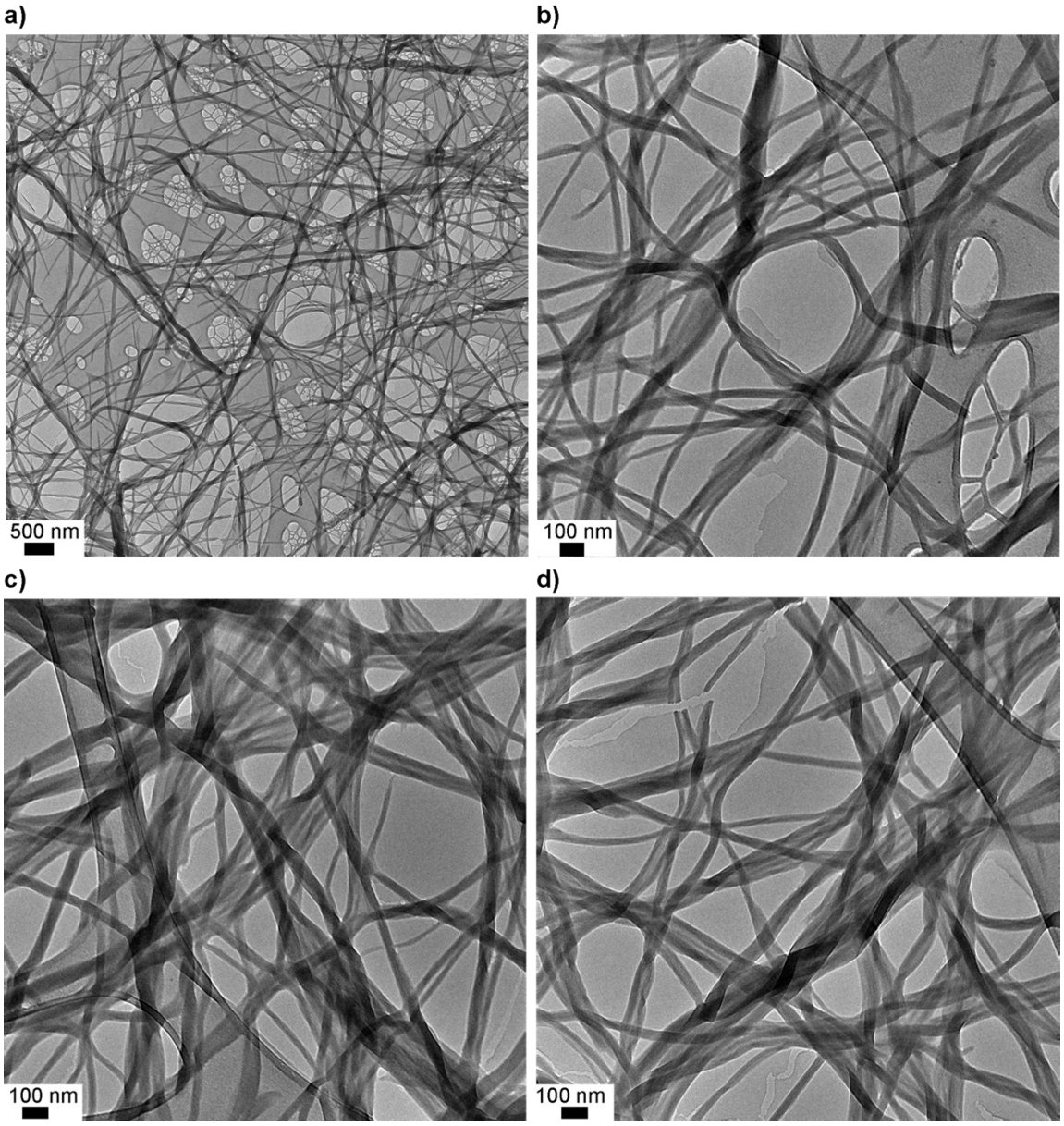

Figure S18. Transmission electron microscopy. TEM micrographs of aerogels obtained from 1.0 % DMF gels of **1.**

Rheological Measurements

Oscilatory rheological measurements were carried out using AR2000 stress-controlled rheometer (TA Instruments) with a 20 mm steel plate-plate geometry and a Peltier heat plate. The premade gel samples were placed (scooped) on the rheometer and the sample was covered with a sealing lid to prevent the solvent evaporation. Measurements were performed using oscillation frequency of 6.283 rad/s and 20 °C unless otherwise stated. The linear viscoelastic region for oscillatory measurements were confirmed with stress and strain sweeps experiments. Time sweep measurements were perofrmed for 15 minutes at 0.1 Pa to confirm the stability of the gels. Frequency sweeps were carried out in DMSO at 0.1 Pa and in DMF at 0.02 % due to the optimal signal depends on the sample. Step-strain experiments were performed with controlled strain of 0.1 % and 150 % were cycled for 60 s, respectively. Temperature ramps from 20 °C to 90 °C and from 90 °C to 20 °C were measured with 0.1 % strain amplitude and 5 °C/min heating rate. Temperature ramps and step-strain experiments present the average of two measurements. All other experimenst were acquired in triplicates and reported as average. Standard deviations of measurements are presented in the supporting figures below. It should be noted that the DMF gels of 1 are not as robust as those of DMSO gels. At the end of the measurements a clear indication of solvent exclusion was observed.

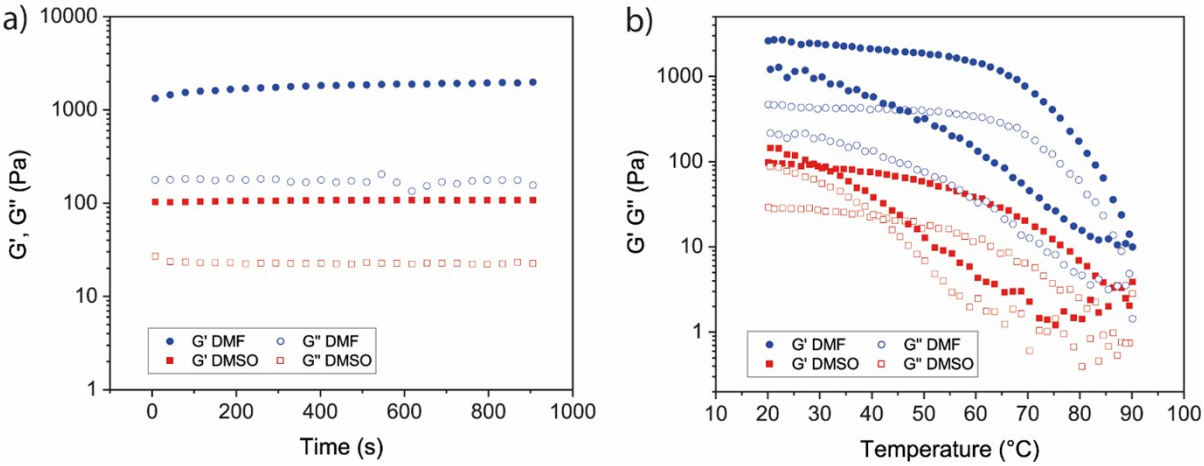

Figure S19. Rheology of 1.0 % DMSO and DMF gels of **1**. Measurements were performed using oscillation frequency of 6.283 rad/s. a) Time sweep measurements with 0.1 Pa stress amplitude showing that the gels are stable at 20 °C. b) Temperature ramp measurements from 20 °C to 90 °C and from 90 °C to 20 °C with 0.1 % strain amplitude and 5 °C/min heating rate.

References

1 R. Tatikonda, S. Bhowmik, K. Rissanen, M. Haukka and M. Cametti, *Dalt. Trans.*, 2016, **45**, 12756–12762.

2 J. H. Price, A. N. Williamson, R. F. Schramm and B. B. Wayland, *Inorg. Chem.*, 1972, **11**, 1280–1284.

3 G. Arena, G. Calogero, S. Campagna, L. Monsù Scolaro, V. Ricevuto and R. Romeo, *Inorg. Chem.*, 1998, **37**, 2763–2769.

4 Agilent, *CrysAlisPro*, Agilent Technologies Inc, Yarnton, Oxfordshire, England, 2013

5 L. Palatinus and G. Chapuis, *J. Appl. Crystallogr.*, 2007, **40**, 786–790.

6 G. M. Sheldrick, *Acta Crystallogr. Sect. C*, 2015, **71**, 3–8.

7 C. B. Hübschle, G. M. Sheldrick and B. Dittrich, *J. Appl. Crystallogr.*, 2011, **44**, 1281–1284.

8 T. Hasegawa, T. Shimoaka, N. Shioya, K. Morita, M. Sonoyama, T. Takagi and T. Kanamori, *Chempluschem*, 2014, **79**, 1421–1425.

9 T. Hasegawa, *Chem. Rec.*, 2017, **17**, 903–917.

10 T. Shimoaka, H. Ukai, K. Kurishima, K. Takei, N. Yamada and T. Hasegawa, *J. Phys. Chem. C*, 2018, **122**, 22018–22023.